ELSEVIER

Biophysical Chemistry 94 (2001) 219–236

Biophysical Chemistry

www.elsevier.com/locate/bpc

Raman spectroscopy of an O_2–Co(II)bleomycin–calf thymus DNA adduct: alternate polymer conformations

Cynthia Rajani[a], James R. Kincaid[b], David H. Petering[a,*]

[a]*Department of Chemistry, University of Wisconsin–Milwaukee, P.O. Box 413, Milwaukee, WI 53211, USA*
[b]*Todd Wehr Chemistry, Marquette University, 535 North 14th Street, Milwaukee, WI 53223, USA*

Received 10 September 2001; received in revised form 11 October 2001; accepted 11 October 2001

Abstract

Bleomycin (Blm) is an antitumor agent which binds to specific sequences of DNA and as HO_2–Fe(III)Blm causes single and double strand cleavage. In the present investigation, binding of O_2–Co(II)Blm to a native DNA polymer, calf thymus DNA, was examined using conventional Raman spectroscopy. O_2–Co(II)Blm is a model for O_2–Fe(II)Blm, the direct precursor of HO_2–Fe(III)Blm. Although the DNA polymer retained a predominant B-form structure, Raman spectral evidence was obtained for localized structural changes to A, C and Z-DNA forms. The presence of these alternate DNA forms within B-DNA implied the presence of B/A, B/C and B/Z junctions. The observed changes in DNA secondary structure were attributed to perturbation of structural water resulting from binding of O_2–Co(II)Blm within the minor groove.

Keywords: Bleomycin; Calf thymus DNA; Raman spectroscopy

1. Introduction

Bleomycin (Blm) constitutes a family of antineoplastic glycopeptide natural products which are isolated from *Streptomyces verticillus* [1–3]. The administered form of the drug is known as Blenoxane and contains bleomycins A_2 and B_2 which differ only in the structure of their respective R-groups (Fig. 1). Although the drug was originally isolated as a mixture of Blm and CuBlm, it has been established that Fe is the necessary cofactor for the cytotoxic effects of the drug [4,5]. Upon coordination of Fe(II), an O_2–Fe(II)Blm complex quickly formed [6]. Two equivalents of this complex then undergo a reaction to generate the activated form of the drug, HO_2–Fe(III)Blm [7].

$$Fe^{2+} + Blm \rightleftarrows Fe(II)Blm \quad (1)$$

$$Fe(II)Blm + O_2 \rightleftarrows O_2\text{–}Fe(II)Blm \quad (2)$$

$$2O_2\text{–}Fe(II)Blm + H^+ \rightleftarrows HO_2\text{–}Fe(III)Blm + Fe(III)Blm + O_2 \quad (3)$$

Iron–bleomycin has the ability to bind preferentially to double-stranded helical DNA and as HO_2–Fe(III)Blm to effect both single and double

* Corresponding author. Tel.: +1-414-229-5853; fax: +1-414-229-5530.
E-mail address: petering@uwm.edu (D.H. Petering).

0301-4622/01/$ - see front matter
PII: S0301-4622(01)00237-X

strand DNA cleavage at specific 5′-GC/T-3′ sites [8–11].

Co(II)Blm does not activate dioxygen to react with DNA, but it does bind O_2 and has been used as a model for the O_2–Fe(II)Blm complex [12,13]. ESR studies have determined that the single, unpaired spin of O_2–Co(II)Blm resides largely on the dioxygen ligand so that the electronic structure approaches O_2^-–Co(III)Blm [14]. ESR spectra of O_2–Co(II)Blm bound to DNA fibers indicate that orientation of the O–O bond is constrained in a plane that is perpendicular to the DNA fiber axis [15]. From this result, it has been inferred that the coordination site of cobalt is sterically fixed with respect to DNA. It was proposed that interactions between the metal domain and the DNA structure contribute to this highly ordered structure. Stability of the dioxygenated cobalt complex toward dimerization as in reaction (3) is achieved through DNA binding as the ratio of calf thymus DNA base

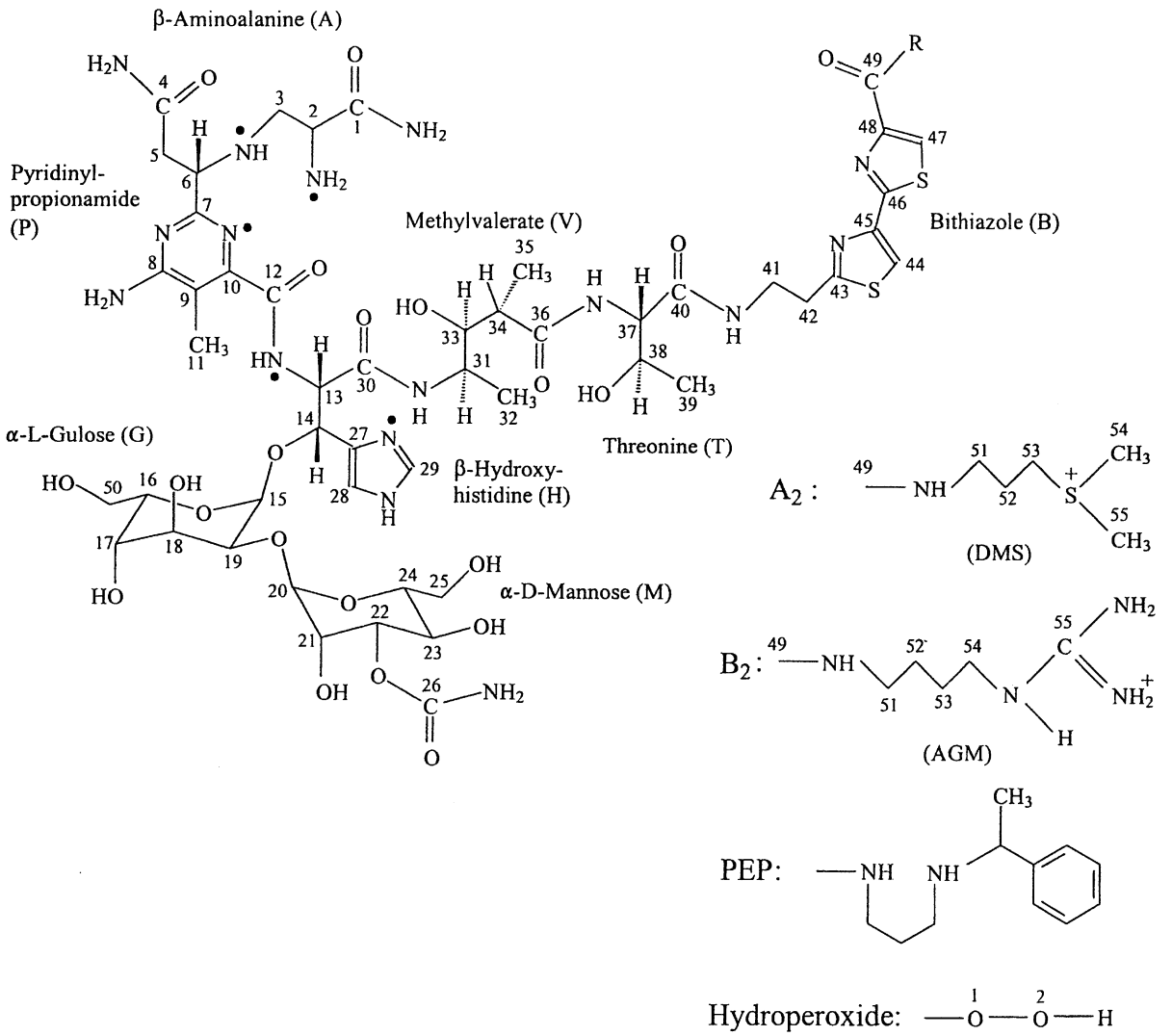

Fig. 1. The structure of metal-free bleomycins A_2 and B_2. Dots indicate ligands that are hypothesized to bind Co(II) in O_2–Co(II)Blm.

pairs: O_2–Co(II)Blm is increased; at a ratio of 10:1, O_2–Co(II)Blm has been found to be stable for at least 24 h [13]. Significant stabilization of the O_2–Fe(II)Blm complex occurs at 25:1 DNA base pairs:Blm [16].

The stability and diamagnetic character of the final products shown in reaction 3 for the analogous cobalt structures, Co(III)Blm and HO_2–Co(III)Blm, have allowed detailed ^{1}H-NMR studies of these complexes to be performed. The metal domain and peptide linker of both these complexes fold into a globular structure [17,18]. Extending below the axial, hydroperoxide binding site is the bithiazole moiety. Each complex has the same chirality and binds specifically in slow exchange on the NMR time scale to oligomers containing 5′-GC/T-3′ specific sites [19–21].

NMR structural analysis of HO_2–Co(III)Blm–A_2 bound to d(CCAGGCCTGG)$_2$ has clearly shown that the bithiazole-tail of this structure fully intercalates between the base pairs that include C6 and C7 [21]. The metal domain-peptide linker unit of both cobalt bleomycin structures binds within the minor groove with the pyrimidinyl N3 and 4-amino groups forming specific H-bonds with the N3 and 2-amino group, respectively, of G5 within the DNA duplex.

Examination of the structure of HO_2–Co(III)Blm–A_2 bound to the DNA oligomer, d(GGAAGCTTCC)$_2$, indicates that the geometric orientation of the metal domain of this structure is similar to that of O_2–Co(II)Blm oriented on salmon sperm DNA fibers, as determined by EPR spectroscopy [22]. This similarity extends to Fe(III)Blm and NO–Fe(II)Blm associated with oriented salmon sperm DNA fibers [22]. These results, coupled with the similarity between the reactions of the dioxygenated Fe and CoBlm species in solution, support the hypothesis that O_2–Co(II)Blm–DNA is an excellent model system for O_2–Fe(II)Blm–DNA.

The interest and need to examine the properties of O_2–Co(II)Blm and O_2–Fe(II)Blm bound to DNA stem from the strong inference that Fe(III)Blm is activated to HO_2–Fe(III)Blm while bound to DNA. Thus, upon exposure of cells to drug, only a small fraction of it becomes associated with DNA in the nucleus [23]. It is likely that this is the reactive pool of drug with DNA both because of its proximity to the polymer and because HO_2–Fe(III)Blm in solution turns over very rapidly causing self-inactivation [7,24]. In addition, Fe(III)Blm can be activated directly in the nucleus by NADH and NADPH [25].

Previous structural work on metallobleomycins has been performed using small synthetic oligomers which were designed to contain either specific (GC) and nonspecific (AT) binding sites [19–21,26]. As such, these small pieces of DNA did not contain sequences that were both amenable and long enough to stabilize the formation of alternate double helical conformations [27–29]. In the present study, conventional Raman spectroscopy was used to examine the structural consequences of binding O_2–Co(II)Blm to native calf thymus DNA. Because calf thymus DNA contains a large variety of base sequences, the possibility of alternate modes of drug binding and drug-

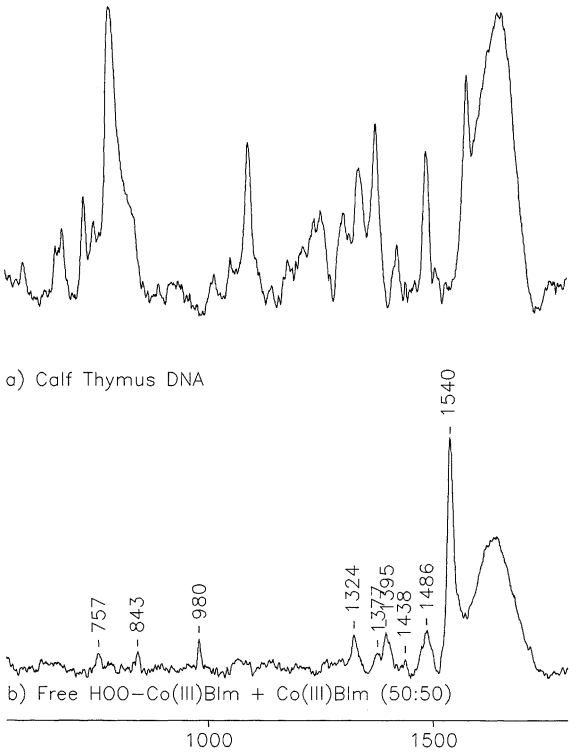

Fig. 2. The absolute Raman data for DNA (35 mM base pairs) and drug (3 mM) which is not bound to DNA.

induced DNA secondary structural perturbations could be investigated. In particular, the experiments demonstrate localized B→A and B→Z changes in DNA conformation as a result of O_2–Co(II)Blm binding. This investigation reveals significant differences between the interactions of O_2–Co(II)Blm and metal-free bleomycin with DNA [30,31].

2. Experimental

2.1. Sample preparation

Calf thymus DNA was purchased from Sigma–Aldrich (Milwaukee, WI) and was used without further purification. A 2.5% solution of DNA was prepared in 0.02 M Tris buffer, pH 7.5/0.1 M NaCl. The solution was sonicated at 4 °C at a low setting for 15–20 min and then rapidly filtered using a 0.2-μM syringe filter. The resulting somewhat viscous solution was clear and particle-free. Concentrations were determined using UV spectrophotometry, $\epsilon_{257}=13.2$ cm^{-1} mM^{-1}/base pair [30–32]. Bleomycin sulfate was purchased from Sigma (St. Louis, MO) and was used as the mixture of Blm A_2+B_2 without further purification. The concentration of Blm was determined using UV–vis spectrophotometry, $\epsilon_{290}=14.0$ cm^{-1} mM^{-1} [21,30].

Initially, the Raman spectrum of DNA alone was measured and found to be consistent with calf thymus DNA Raman spectra done by other workers in the field [33–35]. Then this same DNA solution was used to prepare samples of Blm–DNA which had a 1:10 ratio of drug to base pairs; the final concentration of Blm was 3.0 mM while that of DNA was 30 mM base pairs ($\epsilon_{257}=13.2$ cm^{-1} mM^{-1}/base pair) [32]. Subsequently, 0.9 equivalents of Co^{2+}, dissolved in 5.0 μl of deionized water, was added to the Blm–DNA sample. The final solution was mixed gently in the NMR tube over an extended period to fully dioxygenate the drug. The quality of the samples was checked before and after Raman measurements using UV–vis spectrophotometry (1:200 dilution). The small addition volumes of both drug and Co^{2+} solutions were such that the concentration of solvent was nearly constant among all samples, including DNA, Blm–DNA and O_2–Co(II)Blm–DNA. Therefore, solvent corrections were not needed for the Raman spectra.

2.2. Raman spectroscopy

Raman spectra were measured on a Spex model 1403 double monochromator coupled with a Hamamatsu R-928 photomultiplier and a Spex DM1B data station. Excitation at 514.5 nm was done using a Spectraphysics Ar^+ laser model 2025-05. First, calf thymus DNA was measured, followed by Blm–DNA after addition of drug. Lastly, Co^{2+} was added to Blm–DNA to form O_2–Co(II)Blm–DNA. Multiple scans were taken of each sample; each spectrum was checked for discrepancies and then were subsequently added to produce the final spectral results. Each sample was scanned for 10 h in a spinning NMR tube in order to avoid localized sample heating. The scattered light was collected using a 135° backscattering geometry. The laser power at the sample was 400 mW. The temperature was measured before and after each 30-min scan and was the reported temperature ±0.5 °C.

2.3. Deconvolution procedure

The impact of drug binding on DNA can be visually estimated from the Raman difference spectrum, (drug–DNA minus free drug). In order to obtain more refined information about perturbations of polymer structure, Raman spectra have been curve fit based on extensive information derived from previous UVRR studies and conventional Raman/curve-fitting analyses of both model compounds and DNA [28–31,33–50]. Spectracalc® software (Galactic Industries) was used to deconvolute spectra employing a procedure which has been described earlier [30,31]. The Raman spectral contributions of metal-free Blm were less than 10% in the spectral regions of interest and, therefore, were not subtracted from the Blm–DNA spectrum. Only when Blm was coordinated with Co^{2+} was there evidence of any Raman bands attributable to the drug (>10% above noise level) in the drug-DNA spectrum. Two very weak bands centered at 757 and 843 cm^{-1} in the low frequency

region as well as a stronger band centered at 1486 cm^{-1} were subtracted from the drug–DNA composite spectrum in order to obtain a spectrum of O_2–Co(II)Blm perturbed DNA.

A two-point baseline correction on either end of the spectrum and another 10 point baseline correction were made on the final accumulated spectrum for each sample. Care was taken to correct the baseline in regions containing no spectral features. Exactly the same correction points were selected for each sample. This procedure eliminated any possibility of artifactual difference features in the difference spectrum which may result from slight variations in the baselines. The term 'absolute Raman spectrum' is used here to distinguish spectra treated as described above from the 'difference' spectrum obtained by subtracting the Raman spectrum of the Co(III)Blm+HO_2–Co(III)Blm from that of O_2–Co(II)Blm–DNA as described below. The difference spectrum was smoothed by 5%; no changes in band shape, intensity or frequency resulted from this procedure.

Resonance Raman spectra of HO–Co(III)Blm, HO_2–Co(III)Blm, and Co(II)Blm are essentially identical in the mid-frequency range (data not shown). Raman modes of these complexes are very similar to those of the Fe(II) and Fe(III)Blm complexes in the high/mid-frequency regions [51]. The only modes which appear in the low frequency region are those associated with the dioxygenated species, i.e. ν(Co–O) and ν(O–O) (unpublished results) and a few weak modes in the region 750–845 cm^{-1}. It was, therefore, assumed that the mid-frequency spectrum of O_2–Co(II)Blm was identical with that of the other CoBlm complexes. In the previous resonance Raman study of Fe(II)Blm and CO–Fe(II)Blm bound to $d(CGCGCG)_2$ and $d(ATATAT)_2$, the modes of the drug were unchanged (± 1 cm^{-1}) upon binding to DNA [51]. The choice of 514 nm as the laser wavelength employed for excitation in the present study ensured that none of the drug modes would be resonance enhanced resulting in drug bands were very weak in the Raman spectrum. The only strong non-resonant mode associated with the drug is the isolated bithiazole mode at 1540 cm^{-1} (Figs. 2 and 3). Based on this range of experience with the drug, subtraction of the

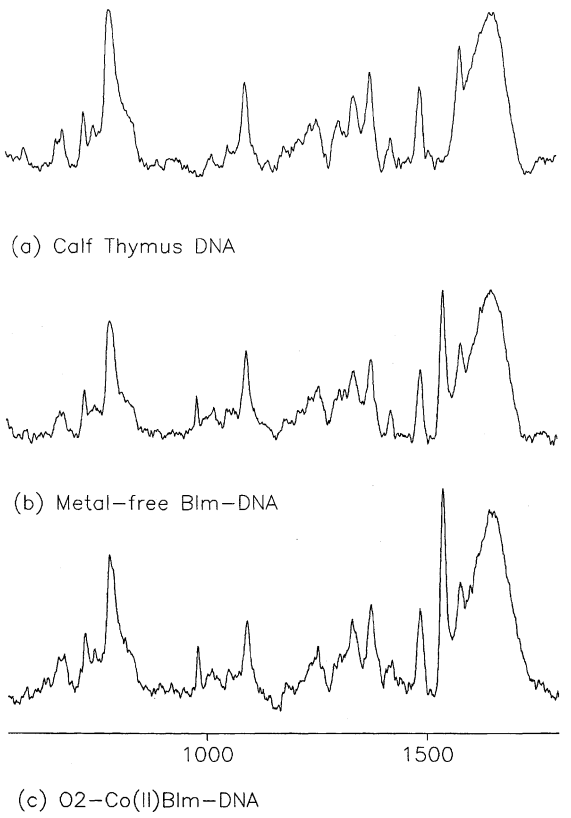

Fig. 3. The absolute Raman data for the entire recorded region for DNA, the Blm–DNA complex and the O_2–Co(II)Blm–DNA complex before subtraction of the drug contribution to the spectrum.

Raman spectrum of the mixture of HO_2–Co(III)Blm plus Co(III)Blm from the O_2–Co(II)Blm–DNA spectrum was considered to result in a difference spectrum representing drug-perturbed DNA modes. The contributions to the spectrum from the drug were digitally subtracted from the spectrum of the drug–DNA complex using the 1540 cm^{-1} band as the reference.

The band frequencies and bandwidths used in the curve fitting procedure were derived from previous UVRR and conventional Raman studies of various DNA oligomers as well as natural DNA from a variety of sources [32,33,38–53]. As a result of the extensive information regarding these spectral parameters available in the literature, a clear understanding exists on how many bands

occur in each region, as well as their assignments. The value for the spectral parameters are listed above. These literature data were employed to generate the spectral parameters for the model compounds (a) Poly (dG)–Poly (dC) and (b) Poly (dA–dT)–Poly (dA–dT). The relative intensities as well as bandwidths and band frequencies for calf thymus DNA were derived using a specific ratio [~55%/45% of (a)/(b)] and also from UVRR studies of this native DNA [53]. This information was subsequently used as a first approximation to fit the drug-perturbed DNA spectrum [30,31]. A 50%/50% Lorentzian/Gaussian band shape was assumed and fixed for all the bands [36,49]. The quality of fit was determined both by visual inspection and examination of the final chi-squared (χ^2) value, resulting from the deviations between simulated and experimental data. Previous assignments of bands were then used to identify the comparable bands in the spectra presented here.

3. Results

3.1. Introduction

The absolute Raman spectra of calf thymus DNA, Blm–DNA and O_2–Co(II)Blm–DNA are shown in Fig. 3. A Raman spectral comparison between DNA (Figs. 4–6a), Blm–DNA (Figs. 4–6b) and O_2–Co(II)Blm–DNA (Figs. 4–6c) was performed in the regions 575–880, 1400–1525 and 1165–1280 cm^{-1}. It was only in the mid-frequency region, 1400–1525 cm^{-1}, of the O_2–Co(II)Blm–DNA spectrum that a band from the drug of significant intensity was observed at ~1486 cm^{-1}. This mode was also found in the spectra of HO_2–Co(III)Blm and HO–Co(III)Blm at this frequency (data not shown). A similar band is present in spectra of related CO–Fe(II)Blm and Fe(III)Blm complexes and does not shift upon binding to DNA [51].

The Raman spectrum of the drug was digitally subtracted from the drug–DNA spectrum, using the well-resolved drug band at 1540 cm^{-1} as the internal reference (Fig. 3c). There is an excellent coincidence of the absolute (Figs. 4–6a,b) and difference (Figs. 4–6c) spectra with their curve fit

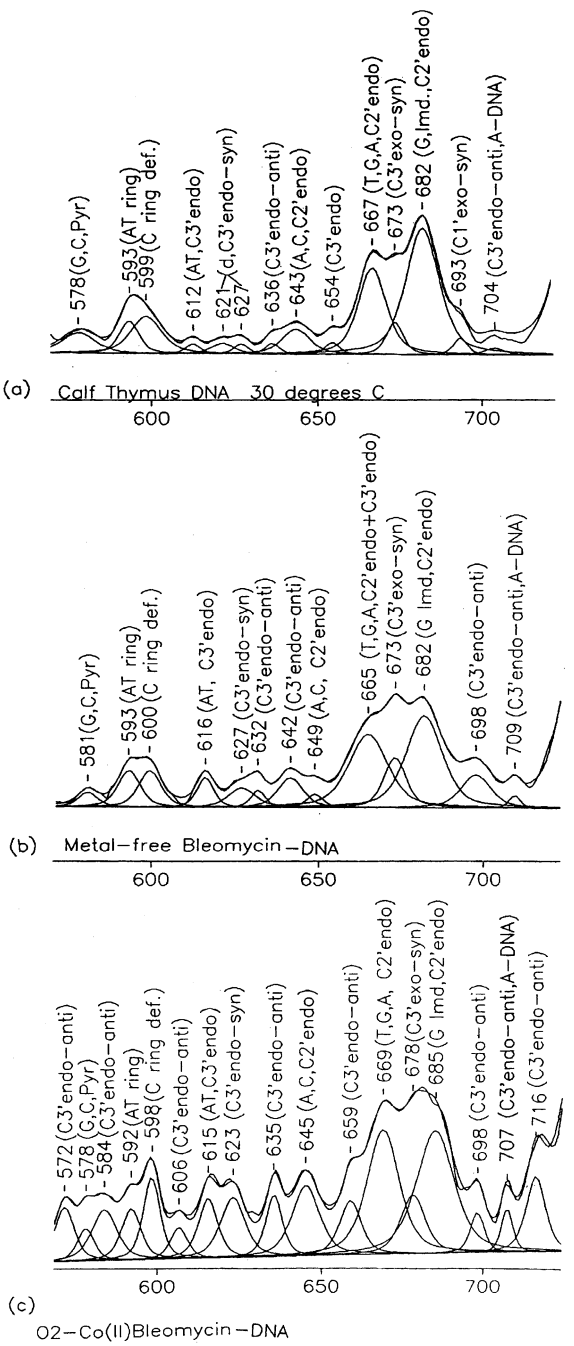

Fig. 4. Absolute Raman spectra of DNA (a) and Blm–DNA (b), and difference Raman spectrum of O_2–Co(II)Blm–DNA (c) as well as the deconvolution results for the spectral region 570–720 cm^{-1}.

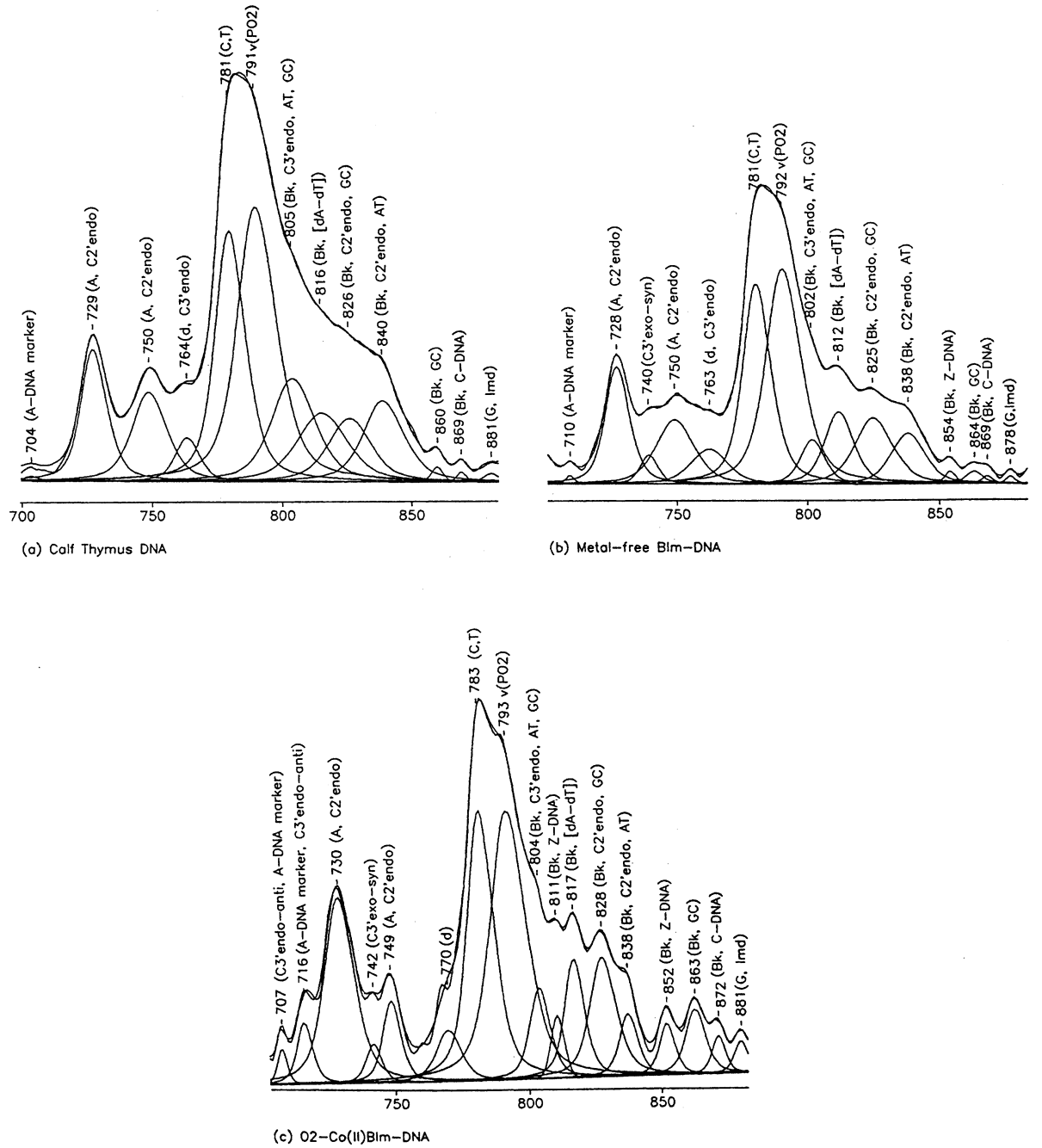

Fig. 5. Absolute Raman spectra of DNA (a) and Blm–DNA (b), and difference Raman spectrum of O_2–Co(II)Blm–DNA (c) as well as the deconvolution results for the spectral region 700–880 cm^{-1}.

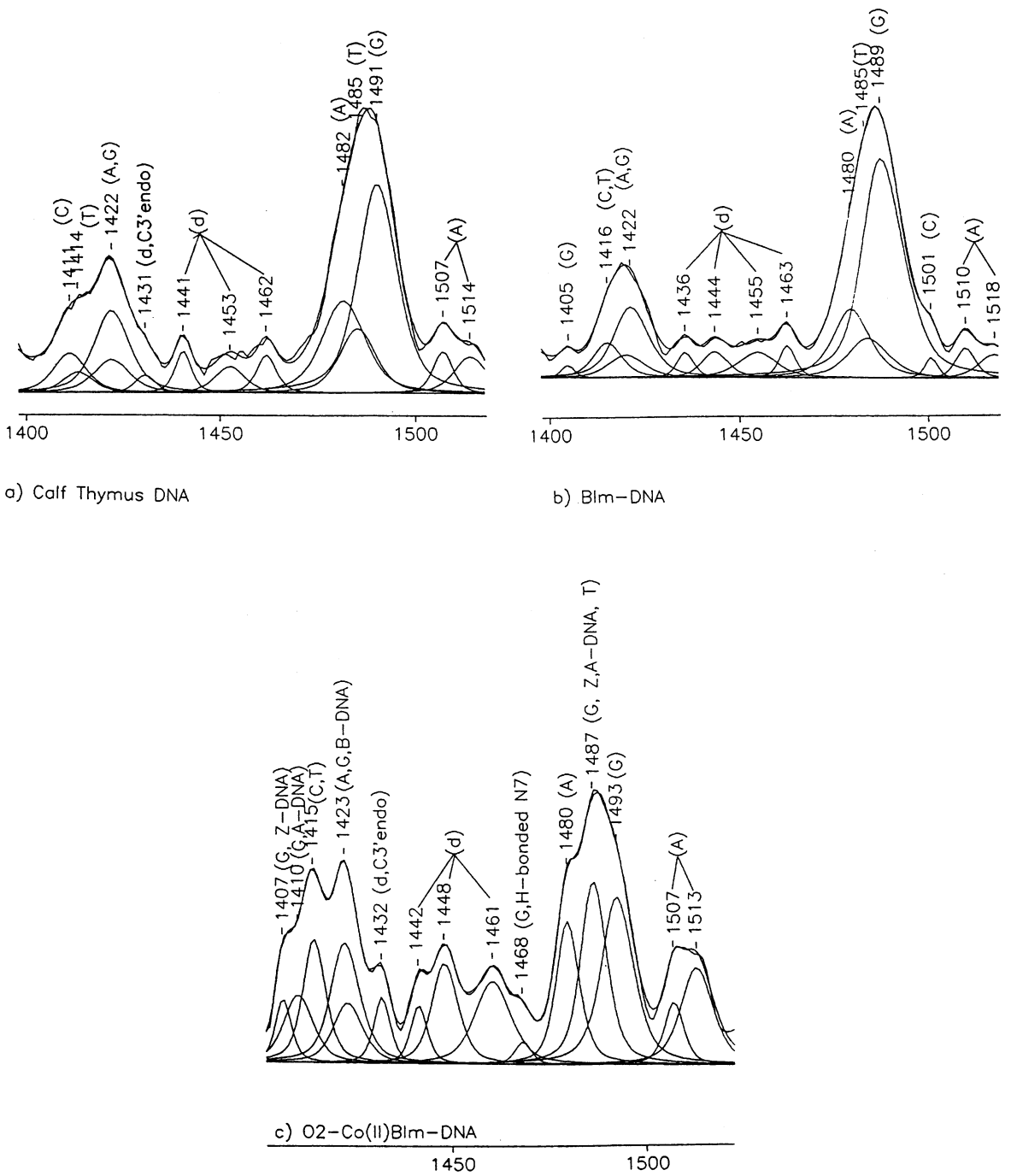

Fig. 6. Absolute Raman spectra for DNA (a) and Blm–DNA (b), and difference Raman spectrum of O_2–Co(II)Blm–DNA (c) as well as the deconvolution results for the spectral region 1400–1525 cm^{-1}.

counterparts. Although most of the bands are readily observed in the absolute and Raman difference spectrum, they are more clearly visualized using the curve fitting analysis. The quantitative results are listed in Table 1 [30,31,37,53]. The fitting parameters for the bands relevant to the present discussion are listed in Table 2.

The spectra in Fig. 4a–6a for DNA alone were deconvoluted using only the modes of known frequencies and bandwidths obtained from previous studies. The curve fitting protocol generated the final deconvolutions without the need to vary either the band position or width. Upon addition of Blm or O_2–Co(II)Blm to DNA, deconvolutions required changes in band frequency and bandwidth as well as the inclusion of other modes.

3.2. Raman spectral evidence for B→Z and B→A transitions in the O_2–Co(II)Bleomycin–DNA complex: low frequency Raman spectral region, 570–720 cm^{-1}

Fig. 4a–c shows the absolute Raman spectra of DNA and Blm–DNA along with the difference spectrum for O_2–Co(II)Blm–DNA for the region 570–720 cm^{-1}. An important feature consistent with the presence of Z-DNA structure within O_2–Co(II)Blm–DNA was observed at 623 cm^{-1}. Based on previous Raman studies of Z-DNA, this mode was assigned to a furanose ring in the C3′*endo–syn* conformation typical of Z-DNA [38,40,41].

There are four bands centered at 572, 584, 606 and 716 cm^{-1}, which appear only upon the binding of O_2–Co(II)Blm to DNA (Fig. 4c). All have been assigned to C3′*endo–anti* deoxyribose modes, a furanose conformation associated with A-DNA structure [49,50]. Additional evidence of a B→A local transition consists of the appearance of a shoulder at 659 cm^{-1} coupled with an increase in the intensity of a band at 635 cm^{-1}, that are also assigned to C3′*endo–anti* furanose vibrations. Previously, Thomas and co-workers demonstrated that in the B→A DNA transition, the 667 cm^{-1} band downshifts and splits into two bands, representing C3′*endo* furanose conformations of A-DNA, one appearing at ~660 cm^{-1} and the other in the region of ~640 cm^{-1} [50]. The band at 707 cm^{-1}, an A-DNA marker band, also appears more intense in comparison with the corresponding band in DNA and Blm–DNA complex. Another A-DNA marker band was detected at 716 cm^{-1} in the spectrum of O_2–Co(II)Blm–DNA [29,33,40,50].

3.3. Low frequency Raman spectral region, 720–880 cm^{-1}

DNA backbone marker bands are associated not only with the nucleotide bases but also with the deoxyribose-phosphate backbone of the DNA polymer and are, therefore, sensitive to conformational changes in secondary structure (Fig. 5) [40,41,43,49]. The backbone marker region of B-DNA, 800–880 cm^{-1}, has been analyzed extensively in previous studies of model compounds and other natural DNAs and is known to contain 7 bands which were found in the present analysis [29,31,40,44–50]. Fig. 5a–c displays the spectral region, 720–880 cm^{-1}, for DNA, Blm–DNA, and O_2–Co(III)Blm–DNA. In comparison with the spectrum of DNA, it can be seen that the bands in the spectra of Blm–DNA and O_2–Co(II)Blm–DNA become progressively more resolved as a result of bandwidth narrowing.

A mode that occurs only in the Raman spectrum of the O_2–Co(II)Blm–DNA adduct is partially resolved in the absolute spectrum at 811 cm^{-1} (Fig. 5c). This band has been assigned as a DNA backbone marker mode for Z-DNA, (C3′*endo–syn*) [40,41,43,49]. Another indication of the Z–DNA structure in this adduct is the large increase in another Z-DNA backbone marker band at 852 cm^{-1} compared to the other structures [40,41,46,54].

Upon binding of Blm to DNA (Fig. 5b), the backbone vibration at 802 cm^{-1} (assigned to AT, GC base pairs, C3′*endo*) narrowed by 9 cm^{-1} in comparison with DNA and became markedly Raman hypochromic ($I/I_{DNA}=0.44$), presumably, due to intercalation of the bithiazole moiety between the DNA base pairs (Fig. 5a) [30,31]. The binding of O_2–Co(II)Blm resulted in further narrowing by 2 cm^{-1} and increased intensity ($I/I_{DNA}=0.71$) and area (27%) relative to the Blm–

Table 1
Changes in the Raman spectral parameters of metal-free bleomycin/DNA and O_2–Co(II)bleomycin/DNA relative to DNA (data collected at 30 °C)

DNA[a]	Blm[a]	$\Delta\nu$[b]	Δbw[c]	I/I_{DNA}[d]	CoBlm	$\Delta\nu$	Δbw	I/I_{DNA}	Assignment[e]
–	–	–	–	–	572/9	–	–	–	d, C3′*endo*–*anti*
578/12	581/7	+3	−5	0.69	578/13	NC[h]	NC	1.00	G, C Pyr ring
–	–	–	–	–	584/9	–	–	–	d, C3′*endo*–*anti*
593/7	594/8	NC	NC	1.00	592/7	NC	NC	1.41	AT ring
599/11	600/8	NC	−4	1.00	598/6	NC	−5	1.00	C ring def.
–	–	–	–	–	606/6	–	–	–	d, C3′*endo*–*anti*
613/5	616/6	+3	NC	2.85	615/7	NC	NC	5.44	AT,C3′*endo*
622/8	–	–	–	–	623/9	NC	NC	5.16	d, C3′*endo*–*syn*
636/5	632/5	−4	NC	1.50	635/6	NC	NC	5.05	d, C3′*endo*–*anti*
644/10	642/9	NC	NC	1.00	645/10	NC	NC	2.49	A, C C2′*endo*
655/5	649/6	−6	NC	1.00	659/8	+4	+3	4.10	d, C3′*endo*
667/10	665/14	NC	+4	0.80	669/12	NC	NC	0.92	T, G, A C2′*endo*
674/6	673/8	NC	NC	1.45	678/9	+4	+3	1.62	d, C3′*exo*–*syn*
682/12	682/13	NC	NC	0.69	685/14	+3	NC	0.85	G, Imd, C2′*endo*
694/5	698/11	+4	+6	1.84	698/14	+4	+9	2.15	d, C3′*endo*–*anti*
704/7	710/4	+6	−3	1.83	707/4	+4	−3	5.96	d, C3′*endo*–*anti*
–	–	–	–	–	716/7	–	−−	–	d, C3′*endo*–*anti*
729/12	728/11	NC	NC	0.89	730/13	NC	NC	1.14	T ring,C2′*endo*
–	740/8	–	–	–	742/7	NC	NC	1.00[d]	d, C3′*endo*
750/16	750/17	NC	NC	0.72	749/8	NC	−8	(0.37)[c] 0.74	A ring,C2′*endo*
764/11	763/17	NC	+6	0.81	770/11	+6	NC	1.00	d, C3′*endo*
781/14	782/13	NC	NC	0.80	783/12	NC	NC	0.87	C, T
791/18	792/16	NC	NC	0.79	793/16	NC	NC	0.79	$\nu(PO)_2^-$
805/20	802/11	−3	−9	(0.24)[g] 0.44	804/9	NC	−11	(0.33)[g] 0.71	C3′*endo* GC, AT
–	–	–	–	–	811/6	–	–	–	Bk, Z-DNA
816/23	813/13	−3	−10	(0.60) 0.00	818/9	NC	−14	(0.55) 1.38	AT Bk
826/20	826/17	NC	−3	(0.90) 1.00	828/12	NC	−8	(0.91) 1.51	Bk, C2′*endo*, GC
840/19	839/15	NC	−4	(0.50) 0.64	838/8	NC	−11	(0.27) 0.62	Bk, C2′*endo*, AT
–	854/5	–	–	–	852/7	NC	NC	3.12[f]	Bk, C3′*endo*–*syn*
860/5	864/8	+4	+3	0.82	863/9	+3	+4	3.32	Bk, GC
870/4	869/5	NC	NC	0.81	872/6	NC	NC	2.94	Bk, C-DNA
881/7	878/4	−3	−3	1.00	881/6	NC	NC	3.07	G, Imd, sugar
–	1405/3	–	–	–	1407/5	NC	NC	4.19[f]	G, (Z-DNA)
1411/10	–	–	–	–	1410/9	NC	NC	1.39[d]	C, (G, A-DNA)[i]
1414/9	1416/9	+2	NC	0.59	1415/7	NC	NC	4.84	T, (C,T)[j]
1422/11	1421/11	NC	NC	0.70	1423/9	NC	NC	1.47	G ($C_4N_9-\delta C_8H$)
1422/11	1422/11	NC	NC	0.87	1423/9	NC	NC	1.18	A ($C_4N_9-\delta C_8H$)
1431/6	1436/5	+5	NC	1.48	1432/5	NC	NC	3.07	d, C3′*endo*
1441/5	1444/8	+3	+3	0.64	1442/5	NC	NC	1.14	C2′H2 def
1453/9	1455/12	NC	+3	1.00	1448/8	−7	NC	3.03	D
1462/6	1463/5	NC	NC	0.87	1461/11	NC	+6	1.77	C5′H2 def
–	–	–	–	–	1468/5	–	–	–	(G, H-bonded N7)
1482/13	1480/12	NC	NC	0.76	1480/7	NC	−6	(0.68) 1.26	A ($\delta C_2H-N_9C_8+\delta C_8H$)
1485/11	1485/13	NC	NC	0.62	1487/8	+2	−3	(1.68) 2.31	T, G (A,Z–DNA)
1491/12	1489/13	NC	NC	1.00	1493/10	+2	−2	0.65	G (B-DNA)
1507/6	1510/3	+3	−3	0.74	1507/6	NC	NC	1.22	A ring
1515/10	1518/10	+3	NC	0.65	1513/10	NC	NC	2.13	A ring

[a] Band center, cm^{-1}/full width of band at half maximum height (FWHM).
[b] Change in frequency relative to DNA.
[c] Change in bandwidth, FWHM, relative to DNA.
[d] Intensity of band compared with intensity of band in DNA.
[e] Refer to Refs. [24,25,28,29,31,32,34,36–38,41–43,46,52] for assignments. Abbreviations: Bk, backbone; d, deoxyribose; def; deformation; δ, bending mode; Imd, imidazole.
[f] Values in parentheses are comparisons of peak areas, A/A_{DNA} for a particular band.
[g] Comparison with Blm–DNA complex.
[h] NC is an abbreviation for 'no change'.
[i] The frequencies are degenerate in CoBlm.
[j] The frequencies are degenerate for C,T in Blm and CoBlm.

Table 2
Changes in the Raman spectral parameters of metal-free bleomycin/DNA and O_2–Co(II)bleomycin/DNA relative to DNA (data collected at 30 °C)

DNA[a]	Blm[a]	$\Delta\nu$[b]	Δbw[c]	I/I_{DNA}[d]	CoBlm	$\Delta\nu$	Δbw	I/I_{DNA}	Assignment[e]
–	–	–	–	–	572/9	–	–	–	d, C3′*endo*–*anti*
–	–	–	–	–	584/9	–	–	–	d, C3′*endo*–*anti*
–	–	–	–	–	606/6	–	–	–	d, C3′*endo*–*anti*
622/8	–	–	–	–	623/9	NC[h]	NC	5.16	d, C3′*endo*–*syn*
636/5	632/5	−4	NC	1.50	635/6	NC	NC	5.05	d, C3′*endo*–*anti*
655/5	649/6	−6	NC	1.00	659/8	+4	+3	4.10	d, C3′endo
704/7	710/4	+6	−3	1.83	707/4	+4	−3	5.96	d, C3′*endo*–*anti*
–	–	–	–	–	716/7	–	–	–	d, C3′*endo*–*anti*
805/20	802/11	−3	−9	(0.24)[f] 0.44	804/9	NC	−11	(0.33)[f] 0.71	C3′*endo* GC, AT
–	–	–	–	–	811/6	–	–	–	Bk, Z-DNA
816/23	813/13	−3	−10	(0.60) 1.00	818/9	NC	−14	(0.55) 1.38	AT Bk
826/20	826/17	NC	−3	(0.90) 1.00	828/12	NC	−8	(0.91) 1.51	Bk, C2′*endo*,GC
840/19	839/15	NC	−4	(0.50) 0.64	838/8	NC	−11	(0.27) 0.62	Bk, C2′*endo*, AT
–	854/5	–	–	–	852/7	NC	NC	3.12[g]	Bk, C3′*endo*–*syn*
860/5	864/8	+4	+3	0.82	863/9	+3	+4	3.32	Bk, GC
870/4	869/5	NC	NC	0.81	872/6	NC	NC	2.94	Bk, C-DNA
–	1405/3	–	–	–	1407/5	NC	NC	4.19[g]	G, (Z-DNA)
1411/10	–	–	–	–	1410/9	NC	NC	1.39	C, (G, A-DNA)[i]
1414/9	1416/9	+2	NC	0.59	1415/7	NC	NC	4.84	T (C,T)[j]
1422/11	1421/11	NC	NC	0.70	1423/9	NC	NC	1.47	G (C_4N_9–δC_8H)
1422/11	1422/11	NC	NC	0.87	1423/9	NC	NC	1.18	A (C_4N_9–δC_8H)
1431/6	1436/5	+5	NC	1.48	1432/5	NC	NC	3.07[f]	d, C3′*endo*
–	–	–	–	–	1468/5	–	–	–	(G, H-bonded N7)
1482/13	1480/12	NC	NC	0.76	1480/7	NC	−6	(0.68) 1.26	A (C_2H–N_9C_8+δC_8H)
1485/11	1485/13	NC	NC	0.62	1487/8	+2	−3	(01.68) 2.31	T, G (A,Z-DNA)
1491/12	1489/13	NC	NC	1.00	1493/10	+2	−2	0.65	G (B-DNA)
1507/6	1510/6	+3	NC	0.74	1507/6	NC	NC	1.22	A ring
1515/10	1518/10	+3	NC	0.65	1513/10	NC	NC	2.13	A ring

[a] Band center, cm^{-1}/full width of band at half maximum height (FWHM).
[b] Change in frequency relative to DNA.
[c] Change in bandwidth, FWHM, relative to DNA.
[d] Intensity of band compared with intensity of band in DNA.
[e] Refer to Refs. [24,25,28,29,31,32,34,36,41–43,46,52], for assignments. Abbreviations include Bk, backbone; d, deoxyribose; δ, bending mode.
[f] Values in parentheses are comparisons of peak areas, A/A_{DNA} for a particular band.
[g] Comparison with Blm–DNA complex.
[h] NC is an abbreviation for 'no change'.
[i] The frequencies are degenerate in CoBlm.
[j] The frequencies are degenerate for C,T in Blm and CoBlm.

DNA complex (Fig. 5c). These differences are consistent with more restricted conformational motion of the O_2–Co(II)Blm–DNA complex than of Blm–DNA and an increase in the population of deoxyribose in the C3′*endo* furanose conformation [44].

The other DNA backbone marker bands of O_2–Co(II)Blm–DNA at 817, 828 and 838 cm^{-1} were also narrowed in relation to Blm–DNA and DNA, indicative of more restricted conformational motion of the DNA polymer when bound to O_2–Co(II)Blm. These results are consistent with the appearance of significant amounts of the A- and Z-DNA conformation in O_2–Co(II)Blm–DNA because these forms are much more rigid than B-DNA [55].

3.4. Mid-frequency spectral region, 1400–1535 cm^{-1}

Fig. 6a shows that there are five bands in the Raman spectral region, 1400–1435 cm^{-1}, of calf thymus DNA. Four of these bands have been observed in UV resonance Raman (UVRR) studies, while the fifth band centered at 1431 cm^{-1} has been assigned previously to a deoxyribose mode in the C3′*endo* furanose conformation typical of A-DNA [40,49,53,55]. The corresponding spectral region of Blm–DNA (Fig. 5b) shows an upshift of the band which was centered at 1411 cm^{-1} in DNA (Fig. 6a) to produce a single band centered at 1416 cm^{-1}. The curve fitting program indicated only one band at 1416 cm^{-1}. Attempts to include two bands close in frequency here resulted in one band with little or no intensity directly beneath the other. Therefore, the band centered at 1416 cm^{-1} was considered to contain contributions from both C and T residues.

In the spectrum of O_2–Co(II)Blm–DNA (Fig. 6c), the five bands and their derived parameters identified in DNA (Fig. 6a) were used as first approximations in the curve fitting analysis for the Raman spectral region 1400–1435 cm^{-1}. The results indicated that there are two degenerate bands at 1423 cm^{-1} (A, G) as well as a band centered at 1415 cm^{-1}, which upon binding of Blm (Fig. 6b) was seen to contain components arising from both C and T residues. Previous UVRR studies have revealed that a mode at 1406 cm^{-1}, assigned to G residues, originates from the G base mode at 1420 cm^{-1} upon conversion of Poly(dG–dC)–Poly(dG–dC) to the Z-DNA form [37]. In the O_2–Co(II)Blm–DNA adduct (Fig. 6c), this band, centered at 1407 cm^{-1}, was increased markedly (fourfold) in intensity relative to Blm–DNA (Table 2, Fig. 6b). Additionally, there was a mode at 1410 cm^{-1} that contained major contributions from G residues in the A-DNA conformation and which also originated from the band centered at 1423 cm^{-1} [40,41,43,53]. Other indications of A-DNA structure, such as a marked increase in the intensity of the deoxyribose mode centered at 1432 cm^{-1} (C3′*endo*, A-DNA), give further support for this assignment.

The 1475–1500 cm^{-1} region of B-DNA includes three bands centered at 1482 (A residues), 1485 cm^{-1} (T residues) and 1490 cm^{-1} (G residues), according to previous UVRR studies of the model compounds, Poly (dA–dT)–Poly (dA–dT), Poly (dG–dC)–Poly (dG–dC) and calf thymus DNA [30,37]. There are also three identifiable bands in this region in the difference spectrum of O_2–Co(II)Blm–DNA (Table 2). The curve fitted band at 1493 cm^{-1} assigned to G, narrowed by 2 cm^{-1}, decreased in intensity ($I/I_{DNA}=0.65$, Table 2) and was slightly upshifted by 2 cm^{-1} compared to DNA. Another band centered at 1487 cm^{-1}, which is assigned to T residues, also upshifted slightly (2 cm^{-1}), narrowed by 3 cm^{-1} and its intensity increased more than twofold with respect to DNA. Previous studies have shown that the 1490 cm^{-1} band in B-DNA undergoes a 5 cm^{-1} downshift in the transition to Z-DNA and a 10 cm^{-1} downshift in the transition to A-DNA [37,40–42]. Therefore, the 1487 cm^{-1} band in the spectrum of the O_2–Co(II)Blm–DNA complex may contain a contribution from G in the Z- and A-DNA conformation along with a contribution from T residues (1485 cm^{-1}) in the B-DNA form. Therefore, the remaining intensity at 1493 cm^{-1} is thought to reflect the intrinsic frequency of G residues in the C2′*endo*, B-DNA conformation. The same reasoning may be applied to the upshift of the 1485 cm^{-1} in DNA to 1487 cm^{-1} with this frequency being closer to that of A- and Z-DNA.

Some of the intensity loss for the band centered at 1493 cm^{-1} in O_2–Co(II)Blm–DNA can also be explained by the appearance of a weak band at 1468 cm^{-1} (Fig. 6c). Based on prior studies, this new mode originates from the 1493 cm^{-1} band and indicates a hydrogen-bond interaction of a bulky ligand, presumably the drug, with N7 (G) [38,39].

Decreases in bandwidths observed for O_2–Co(III)Blm–DNA in this region can be attributed, at least in part, to the presence of both A-DNA and Z-DNA conformations that are much more rigid than that of B-DNA [40,41]. Another possible reason for conformational restriction may be due to the association of the drug with the minor groove of the DNA polymer [21].

3.5. Evidence for the presence of B/Z and B/A junctions in the O_2–Co(II)Bleomycin /DNA complex: low frequency Raman spectral region, 575–880 cm^{-1}

The B-DNA backbone marker modes at 817 cm^{-1} (AT Bk), 828 cm^{-1} (C2′*endo*, GC) and 838 cm^{-1} (C2′*endo*, AT) are partially resolved in the O_2–Co(II)Blm–DNA spectrum and further visualized using curve fitting (Fig. 5c). The fact that a significant amount of band intensity exists for DNA backbone marker bands in the C2′*endo* sugar pucker indicates that much of the polymer is still in the B-DNA conformation. This implies the presence of B/Z, B/C and B/A junctions. An alternative hypothesis is that separate molecules of A, B- and Z-DNA exist in the presence of drug. However, calf thymus DNA contains a heterogeneous array of base pairs and base pair sequences and is a relatively stable polymer with a T_m of ~76 °C 33. These facts weigh heavily against the hypothesis that binding of O_2–Co(II)Blm converts calf thymus B-DNA into uniform alternate conformations.

4. Discussion

The current investigation was conducted at 30 °C, a temperature which has been documented as a midpoint for a 'pre-melt' DNA conformational transition [36,56,57]. Phased $(dA)_5$ tracts in persistence length ($\geq$45 bp) oligomers as well as Poly dA–Poly dT have been shown to exist as two distinct structures. The first is found at a low temperature (<20 °C) where AT base pairs are propeller-twisted so that they can form a third hydrogen-bond and maximal stacking interactions. At higher temperatures (>40 °C), this structure 'melts' into canonical B-DNA in a transition between two discrete states within the double helix [56,57]. DNA intercalative binding of metal-free Blm was favored at 30 °C in comparison with its behavior at 19 °C as indicated by increased Raman hypochromism of most of the vibrational modes of the drug–DNA adduct relative to DNA alone [30].

In the present investigation, binding of O_2–Co(II)Blm to a native DNA polymer, calf thymus DNA, was examined using conventional Raman spectroscopy. Upon coordination of Co(III), HO_2–Co(III), and Zn(II), the metal domain of Blm (Fig. 1) assumes different conformations according to NMR spectroscopy [18,58,59]. As a result, HO_2–Co(III)Blm and ZnBlm bind in the minor groove of small oligomers with different conformations [21,60]. With the former, the bithiazole moiety intercalates into the base pair structure, whereas in ZnBlm it is a minor groove binder. The metal domain interaction with the minor groove may also affect the mode of binding of the bithiazole moiety as a considerable conformational reorganization of the metal domain and peptide linker occurs upon Co(III) coordination [17]. In this context, a study was undertaken to compare perturbations of DNA structure induced by metal-free Blm, which does not have an organized metal domain, and O_2–Co(II)Blm, which is closely related to HO_2–Co(III)Blm.

A- and B-DNA are conformational polymorphs and their formation depends on both DNA sequence and the structural water associated with the DNA polymer [48,54,55]. The energy barrier between C2′*endo–anti* (B-DNA) and C3′*endo–anti* (A-DNA) is very small, particularly under conditions of dehydration, which can be achieved by using higher salt concentrations, alcohol, or some other perturbation of structural water such as drug/protein binding in the minor groove [27,29,31,40,55]. B→Z-DNA transitions are known to be cooperative, to proceed without strand separation, to be sequence selective, and to occur under conditions of high salt and/or low water activity associated with the DNA polymer [55].

The findings of this report are consistent with the appearance of conformational changes in the secondary DNA structure that result from O_2–Co(II)Blm–DNA binding to DNA. Alternative deoxyribose furanose conformations which are characteristic of A-DNA (C3′*endo–anti*) and Z-DNA (C3′*endo–syn*) structures have been detected [40–43,45,49,50,61]. Evidence for B→A and B→Z transitions included changes in frequency and intensity of Raman bands, as well as the appearance of new vibrational bands in the spectrum of O_2–Co(II)Blm–DNA not seen in the spectrum of native DNA structure.

Table 3
A list of DNA sequences that readily form A and Z-DNA conformations [55]

Polynucleotide	Form	Relative humidity (%)
Poly dG–Poly dC	A	75
Poly (dA–dT)–Poly (dA–dT)	Adopts A form only as a metastable state	
Poly dA–Poly dT	Resists any structure except B-DNA	
Poly (dA–dC)–Poly (dG–dT)	A	66
	Z	66
Poly (dG–dC)–Poly (dG–dC)	A	up to 92
	Z	43
Poly (dA–dG–dT)–Poly (dA–dC–dT)	A	up to 98

Previously it was shown that binding of Blm to DNA produced increases primarily in the populations of C3′*endo–anti* furanose conformations, attributable to the interaction between the bithiazole moiety and DNA [31]. The relative increase in populations of A- and Z-DNA markers bands seen with O_2–Co(II)Blm–DNA in comparison with Blm–DNA is consistent with the hypothesis that the metal domain-peptide linker also interacts closely with the DNA bases in the minor groove as previously determined by NMR studies [20,21]. Whether the drug primarily affects base sequence conformation at the site of binding or whether its effects extend significantly beyond this site cannot be assessed by this method.

Above is a short list (Table 3) of DNA sequences which can readily form A- and Z-DNA conformations with Na^+ as a counterion under the designated conditions of relative humidity [56]. What is evident is that alternating 5′-purine/pyrimidine-3′ sequences are most likely to form A- and Z-DNA configurations. Most of them contain 5′-GC/T-3′ sites, which are preferentially cleaved by HO_2–Fe(III)Blm or serve as preferential binding sites of Fe(III)Blm, Co(III)Blm and HO_2–Co(III)Blm [8–12]. This supports the theory that the observed DNA conformational changes are ‘local’ because they result directly from the drug binding at its preferred DNA site.

The results of previous studies of the interaction of Fe(II)Blm complexes with Z-DNA and/or BZ junctions vary. Guo et al. found elevated cleavage at Z-DNA-forming DNA sites even at high salt conditions, suggesting that FeBlm binds preferentially to Z-DNA [62]. Others detected no enhancement of FeBlm DNA cleavage at a BZ junction in high salt concentrations [63]. A third group showed that the presence of FeBlm increased the amount of salt necessary to produce Z-DNA in Poly (dG–dC)–Poly (dG–dC) and, thus, concluded that FeBlm binds preferentially to B-DNA [64]. On the basis of these studies, the nature of the binding and activity of FeBlm with Z-DNA remains ambiguous.

The presence of a band at 1468 cm^{-1} in the Raman spectrum of the O_2–Co(II)Blm–DNA complex signifies an H-bonding interaction of the drug with N7 of G residues. This band originates from the band at $\sim$1490 cm^{-1} [38,39]. Guanine N7 is the most exposed base group in Z-DNA [55]. It has been well documented that the binding of bulky ligands at the N7 of purines strongly stabilizes the *syn* deoxyribose conformation (Z-DNA = C3′*endo–syn*) [39]. Therefore, the binding of O_2–Co(II)Blm may stabilize the Z-DNA conformation at certain sequence-specific regions of DNA via this H-bond interaction.

N7 is also readily accessible to solvent in the major groove of B- and A-DNA. A new NMR structure of HO_2–Co(III)Blm A_2 bound to B-form $d(GGAAGCTTCC)_2$ at the GC base sequence is consistent with hydrogen bond formation between the NH of the amide connecting bleomycinic acid to the R group and guanine N7 opposite C of the recognition site (Fig. 1) (C. Zhao, Q. Mao, C. Xia, H. Försterling, E. DeRose, D.H. Petering, submitted for publication). The present finding bolsters this assignment. It also provides additional Raman evidence for intercalation, since the H-bond formation at N7 infers that a part of the bleomycin structure resides in the major groove. This conclusion is consistent with the insertion of

the R group from the minor groove between base pairs and into the major groove.

In A-DNA the functional group which is most exposed in the minor groove is the 2-amino group of guanine [55]. According to previous reports, the 2-amino group of G of small oligomers containing GC or GT sequences forms an H-bond with the N3 of the pyrimidine ring of Co(III)Blm and HO_2–Co(III)Blm in drug–DNA adducts [21]. Although the dioxygenated species, O_2–Co(II)Blm is not the final HO_2–Co(III)Blm species analogous to activated HO_2–Fe(III)Blm, it contains the major resonance form of O_2^-–Co(III)Blm, which has a charge distribution similar to HO_2–Co(III)Blm [15]. Thus, the B→A transition effected by its interaction with DNA in the minor groove may increase exposure of a key recognition site, the 2-amino group of G.

The prominent population of A-DNA regions observed in this work is consistent with previous experiments which showed that O_2–Co(II)Blm, NO–Fe(II)Blm and Fe(III)Blm establish similarly oriented conformations with respect to A- and B-form salmon sperm DNA [15,22]. The appearance of A-DNA may also rationalize the properties of RNA cleavage by FeBlm since RNA also adopts the A-form conformation. As with its interaction with DNA, HO_2–Fe(III)Blm reacts with RNA species such as transfer RNA at G-pyrimidine sites but with more apparent selectivity in surrounding sequence environment than observed with B form DNA [65,66]. Furthermore, comparison of the reactivity of FeBlm with RNA and DNA molecules with the same sequence, except for U to T substitutions, supports the conclusion that the drug binds more tightly to RNA than DNA [67]. Cleavage occurs in double stranded regions but also within stretches of single stranded RNA and at junctions between single and double stranded polymers [68]. Although, mechanistic understanding of these results is still at a preliminary stage, they show that the drug targets the A-DNA conformation.

The DNA backbone marker bands in the region 800–855 cm^{-1} also revealed that much of the DNA is in the B-DNA form. The sequence heterogeneity of calf thymus DNA precludes the presence of strands of pure A- or Z-DNA conformations. The fact that there are also varying degrees of A- and Z-DNA structures within the DNA polymer implies the presence of BZ and BA junctions. Strong evidence for junctions between different DNA conformations also derives from the presence of mixed sugar pucker conformations and changes in base stacking [55]. Such junctions cause distortions (including unpaired nucleotides) and bending of DNA. For example, the B/Z junction can be formed minimally from one to three GC pairs within a core of twelve or more alternating purine/pyrimidine (either GC or GT) base pairs usually stabilized by flanking A-tracts [33,34,38–47,51–58,69,70]. A stiff bend of the helix axis occurs at the junction. Thus, the observed base unstacking seen with O_2–Co(II)Blm–DNA may be caused, in part, by this conformational deformation.

Non-canonical structures may be important protein and drug recognition sites [71,72]. Williams and Goldberg have detected selective strand scission by FeBlm near DNA bulges which are caused by an unpaired, extra nucleotide on one strand of the double helix [72]. The selectivity of this reaction was considered to be a consequence of stabilized intercalation of the drug at the bulge. Therefore, by analogy, DNA bulges may facilitate intercalation of the bithiazole moiety of O_2–Co(II)Blm.

The increases in intensity seen for many of the vibrational modes of O_2–Co(II)Blm–DNA relative to DNA or Blm–DNA at first suggested the loss of intercalation of the bithiazole moiety, resulting in a decrease in base and drug stacking interactions. However, the interpretation of Raman intensity changes is more complex. Base stacking is an additive effect that is stabilized by weak interactions such as hydrophobic and London dispersion forces. Dipoles, π-electron systems, and dipole-induced dipole moments are all important in this interaction. The most important of these involves dipole-induced dipole interactions whereby the permanent dipole, associated with C=O or C–NH_2 groups are superimposed over the π-electron system of the adjacent base [55]. Thus, as judged by Raman spectroscopy, unstacking of base pairs occurs when the base ring structures and their associated electron density are not oriented to optimize the interaction between transition

dipoles, i.e. the polarization of electrons in a neighboring base by the electrons or permanent dipole in the adjacent base [39,73]. Accordingly, hyperchromism might indicate conformational changes during intercalation which alter the optimal interaction of transition dipoles. Alternatively, it might reflect direct unstacking of bases as occurs at DNA conformer junctions. In this context, the evident formation of B→A and B→Z junctions surely contributes to the observed Raman hyperchromism of multiple bands in the O_2–Co(II)Blm–DNA spectrum.

Acknowledgements

The authors gratefully acknowledge support from NIH grant CA-22184.

References

[1] D.H. Petering, Q. Mao, W. Li, E. DeRose, W.E. Antholine, Metallobleomycin–DNA I: structures and reactions related to bleomycin-induced DNA damage, in: A. Sigel, H. Sigel (Eds.), Metal Ions in Biological Systems, 33, Marcel Dekker, New York, 1996, pp. 619–648.

[2] R.M. Burger, Cleavage of nucleic acids by bleomycin, Chem. Rev. 98 (1998) 1153–1169.

[3] C.A. Claussen, E.C. Long, Nucleic acid recognition by metal complexes of bleomycin, Chem. Rev. 99 (1999) 2797–2816.

[4] H. Umezawa, K. Maeda, T. Tekeuchi, Y. Okami, New antibiotics, bleomycins A and B, J. Antibiot. Ser. A 19 (1966) 200–209.

[5] K. Radtke, F.A. Lornitzo, R.W. Byrnes, W.E. Antholine, D.H. Petering, Iron requirement for cellular DNA damage and growth inhibition by hydrogen peroxide and bleomycin, Biochem. J. 302 (1994) 655–664.

[6] R.M. Burger, J.B. Horowitz, J. Peisach, J.B. Wittenberg, Oxygenated iron bleomycin. A short-lived intermediate in the reaction of ferrous bleomycin with O_2, J. Biol. Chem. 254 (1979) 12999–13002.

[7] R.M. Burger, J. Peisach, S.B. Horwitz, Activated bleomycin: a transient complex of drug, iron, and oxygen that degrades DNA, J. Biol. Chem. 256 (1981) 11636–11644.

[8] L.F. Povirk, W. Wubter, W. Köhnlein, F. Hutchinson, DNA double-strand breaks and alkali-labile bands produced by bleomycin, Nucleic Acids Res. 4 (1977) 3573–3580.

[9] A.D. D'Andrea, W. Haseline, Sequence-specific cleavage of DNA by the antitumor antibiotics neocarzinostatin and bleomycin, Proc. Natl. Acad. Sci. USA 75 (1978) 3608–3612.

[10] M. Takeshita, A.P. Grollman, E. Ohtsubo, H. Ohtsubo, Interaction of bleomycin with DNA, Proc. Natl. Acad. Sci. USA 75 (1978) 5983–5987.

[11] R.J. Steighner, L.F. Povirk, Bleomycin-induced DNA lesions at mutational hot spots: implications for the mechanism of double-strand cleavage, Proc. Natl. Acad. Sci. USA 87 (1990) 8350–8354.

[12] R.X. Xu, W.E. Antholine, D.H. Petering, Reaction of Co(II)bleomycin with dioxygen, J. Biol. Chem. 267 (1992) 944–949.

[13] R.X. Xu, W.E. Antholine, D.H. Petering, Reaction of DNA-bound Co(II)bleomycin with dioxygen, J. Biol. Chem. 267 (1992) 950–955.

[14] Y. Sugiura, Oxygen binding to cobalt(II) bleomycin, J. Antibiot. 31 (1978) 1206–1208.

[15] M. Chikira, W.E. Antholine, D.H. Petering, Orientation of dioxygen bound to cobalt(II) bleomycin–DNA fibers, J. Biol. Chem. 264 (1989) 21478–21480.

[16] P. Fulmer, D.H. Petering, Reaction of DNA-bound ferrous bleomycin with dioxygen: activation versus stabilization of dioxygen, Biochemistry 33 (1994) 5319–5327.

[17] R.X. Xu, D. Nettesheim, J.D. Otvos, D.H. Petering, NMR determination of the structures of peroxycobalt(III) bleomycin and cobalt(III) bleomycin, products of the aerobic oxidation of cobalt(II) bleomycin by dioxygen, Biochemistry 33 (1994) 907–916.

[18] W. Wu, D.E. Vanderwall, S.M. Lui, X.-J. Tang, C.J. Turner, J.W. Kozarich, J. Stubbe, Studies of Co·bleomycin A2 green: its detailed structural characterization by NMR and molecular modeling and its sequence-specific interaction with DNA oligonucleotides, J. Am. Chem. Soc. 118 (1996) 1268–1280.

[19] S.M. Lui, D.E. Vanderwall, W. Wu, X.-J. Tang, C.J. Turner, J.W. Kozarich, J. Stubbe, Structural characterization of Co·bleomycin A2 brown: free and bound to d(CCAGGCCTGG), J. Am. Chem. Soc. 119 (1997) 9603–9613.

[20] Q. Mao, P. Fulmer, W. Li, E.F. DeRose, D.H. Petering, Different conformations and site selectivity of HO_2^-–Co(III)–bleomycin A_2 and Co(III)–bleomycin A_2 bound to DNA oligomers, J. Biol. Chem. 271 (1996) 6185–6191.

[21] W. Wu, D.E. Vanderwall, C.J. Turner, J.W. Kozarich, J. Stubbe, Solution structure of Co·bleomycin A2 green complexed with d(CCAGGCCTGG), J. Am. Chem. Soc. 118 (1996) 1281–1294.

[22] M. Chikira, T. Iiyama, K. Sakamoto, W.E. Antholine, D.H. Petering, Orientation of iron bleomycin and porphyrin complexes on DNA fibers, Inorg. Chem. 39 (2000) 1779–1786.

[23] R.W. Byrnes, J. Templin, D. Sem, S. Lyman, D.H. Petering, Intracellular DNA strand scission and growth inhibition of Ehrlich ascites tumor cells by bleomycins, Cancer Res. 50 (1990) 5275–5286.

[24] J. Templin, L. Berry, S. Lyman, R.W. Byrnes, W.E. Antholine, D.H. Petering, Properties of redox-inactivated bleomycins. In vitro DNA damage and inhibition of Ehrlich cell proliferation, Biochem. Pharmacol. 43 (1992) 614–623.

[25] R.W. Byrnes, D.H. Petering, DNA strand breakage in isolated nuclei subjected to bleomycin or hydrogen peroxide, Biochem. Pharmacol. 48 (1994) 575–582.

[26] P. Fulmer, C. Zhao, W. Li, E. DeRose, W.E. Antholine, D.H. Petering, Fe– and Co–bleomycins bound to site specific and nonspecific DNA decamers: comparative binding and reactivity of their metal centers, Biochemistry 36 (1997) 4367–4374.

[27] A. Pichler, S. Rüdisser, R.H. Winger, K.R. Liedl, A. Hallbrucker, E. Mayer, Nonoriented $d(CGCGAATTCGCG)_2$ dodecamer persists in the B-form even at low water activity, J. Am. Chem. Soc. 122 (2000) 716–717.

[28] J.M. Benevides, G. Chan, X.-J. Lu, W.K. Olson, M.A. Weiss, G.J. Thomas, Protein-directed DNA structure. I. Raman spectroscopy of a high-mobility-group box with application to human sex reversal, Biochemistry 39 (2000) 537–547.

[29] G.A. Thomas, W.L. Kubasek, W.L. Peticolas, P. Greene, J. Grable, J.M. Rosenberg, Environmentally induced conformational changes in B-type DNA: comparison of the conformation of the oligonucleotide d(TCGCGAATTCGCG) in solution and in its crystalline complex with the restriction nuclease *Eco*RI, Biochemistry 28 (1989) 2001–2009.

[30] C. Rajani, J.R. Kincaid, D.H. Petering, The presence of two modes of binding to calf thymus DNA by metal-free bleomycin: a low frequency Raman study, Biopolymers: Nucleic Acid Sci. 52 (1999) 129–146.

[31] C. Rajani, J.R. Kincaid, D.H. Petering, A systematic approach toward the analysis of drug–DNA interactions using Raman spectroscopy: the binding of metal-free bleomycins A_2 and B_2 to calf thymus DNA, Biopolymers: Nucleic Acid Sci. 52 (1999) 110–128.

[32] A. Weselucha-Birczynska, G.D. Strahan, M. Tsuboi, K. Nakamoto, Interaction of bleomycin A_2 with DNA studied by resonance Raman spectroscopy: intercalation or groove binding?, J. Raman Spectrosc. 31 (2000) 1073–1077.

[33] (a) J.M. Benevides, H.-J. Wang, G.A. van der Marel, J.H. van Boom, G.T. Thomas, Crystal and solution structures of the B-DNA dodecamer d(CGCAAATTTGCG) probed by Raman spectroscopy: heterogeneity in the crystal structure does not persist in the solution structure, Biochemistry 27 (1988) 931–938 (b) J.G. Duguid, V.A. Bloomfield, J.M. Benevides, G.J. Thomas, DNA melting investigated by differential scanning calorimetry and Raman spectroscopy, Biophys. J. 71 (1996) 3350–3360.

[34] E. Small, W.L. Peticolas, Conformational dependence of the Raman scattering intensities from polynucleotides. III. Order–disorder changes in helical structures, Biopolymers 10 (1971) 1377–1416.

[35] B. Prescott, W. Steinmetz, G.J. Thomas, Characterization of DNA structures by laser Raman spectroscopy, Biopolymers 23 (1984) 235–256.

[36] S.S. Chan, R.H. Austin, I. Mukerji, T.G. Spiro, Temperature-dependent ultraviolet resonance Raman spectroscopy of the premelting state of dA·dT DNA, Biophys. J. 72 (1997) 1512–1520.

[37] S.P.A. Fodor, R.P. Rava, T.R. Hays, T.G. Spiro, Ultraviolet resonance Raman spectroscopy of the nucleotides with 266-, 240-, 218-, and 200-nm pulsed laser excitation, J. Am. Chem. Soc. 107 (1985) 1520–1529.

[38] J.M. Benevides, T. Li, X.-J. Lu, A.R. Srinivasan, W.K. Olson, M.A. Weiss, G.J. Thomas, Protein-directed DNA structure II. Raman spectroscopy of a leucine zipper bZIP complex, Biochemistry 39 (2000) 548–556.

[39] J.P. Ridoux, J. Liquier, E. Tallandier, Raman spectroscopy of Z-form Poly[d(A–dT)]·Poly[d(A–T)], Biochemistry 27 (1988) 3874–3878.

[40] W.L. Peticolas, E. Evertz, Conformation of DNA in vitro and in vivo from laser Raman scattering, in: D.M.J. Lilley, J.E. Dahlberg (Eds.), Methods in Enzymology, 211, Academic Press, New York, 1992, pp. 335–352.

[41] W.L. Peticolas, Raman spectroscopy of DNA and proteins, in: K. Sauer (Ed.), Methods in Enzymology, 246, Academic Press, New York, 1995, pp. 389–417.

[42] A. Toyama, Y. Takino, H. Takeuchi, I. Harada, Ultraviolet resonance Raman spectra of ribosyl C(1′)-deuterated purine nucleosides: evidence of vibrational coupling between purine and ribose rings, J. Am. Chem. Soc. 115 (1993) 11092–11098.

[43] M. Tsuboi, M. Komatsu, J. Hoshi, E. Kawashima, T. Sekine, Y. Ishido, M.P. Russell, J.M. Benevides, G.J. Thomas, Raman and infrared spectra of (2′*S*)-[2′-2H]thymidine: vibrational coupling between deoxyribosyl and thymine moieties and structural implications, J. Am. Chem. Soc. 119 (1997) 2025–2032.

[44] R.M. Wartell, J.T. Harrell, Characteristics and variations of B-type DNA conformations in solution: a quantitative analysis of Raman band intensities of eight DNAs, Biochemistry 25 (1986) 2664–2671.

[45] G.J. Thomas, J.M. Benevides, S.A. Overman, U. Toyotoshi, K. Ushizawa, M. Saitoh, M. Tsuboi, Polarized Raman spectra of oriented fibers of A DNA and B DNA: anisotropic and isotropic local Raman tensors of base and backbone vibrations, Biophys. J. 68 (1995) 1073–1088.

[46] R.M. Wartell, J.T. Harrell, W. Zacharias, R.D. Wells, Raman spectroscopy study of the B–Z transition in $(dG–dC)_n$·$(dG–dC)_n$ and a DNA restriction fragment, J. Biomol. Struct. Dyn. 1 (1983) 83–96.

[47] Z. Dai, G.A. Thomas, E. Evertz, W.L. Peticolas, The length of a junction between the B and Z conformations in DNA is three base pairs or less, Biochemistry 28 (1989) 6991–6996.

[48] H. DeGrazia, D. Brown, S. Cheung, R.M. Wartell, Solution conformations of DNAs containing binding sites of the catabolite gene activator protein and *lac* repressor protein: characterization by Raman spectroscopy, Biochemistry 27 (1988) 6359–6365.

[49] Y. Nishimura, T. Tsuboi, T. Sato, A. Katsuyuki, Conformation-sensitive Raman lines of mononucleotides and their use in a structure analysis of polynucleotides: guanine and cytosine nucleotides, J. Mol. Struct. 146 (1986) 123–153.

[50] L. Movileanu, J.M. Benevides, G.J. Thomas, Temperature dependence of the Raman spectrum of DNA. Part I—Raman signatures of premelting and melting transitions of Poly(dA–dT)·Poly(dA–dT), J. Raman Spectrosc. 30 (1999) 623–630.

[51] J.W. Sam, S. Takahashi, I. Lippai, J. Peisach, D.L. Rousseau, Sequence-specific changes in the metal site of ferric bleomycin induced by the binding of DNA, J. Biol. Chem. 273 (1998) 16090–16097.

[52] C.A. Grygon, T.G. Spiro, Ultraviolet resonance Raman spectroscopy of distamycin complexes with Poly(dA)–Poly(dT) and Poly(dA–dT): role of H-bonding, Biochemistry 28 (1989) 4397–4402.

[53] S.P.A. Fodor, T.G. Spiro, Ultraviolet resonance Raman spectroscopy of DNA with 200–266-nm laser excitation, J. Am. Chem. Soc. 108 (1986) 3198–3205.

[54] W.L. Peticolas, Z. Dai, G.A. Thomas, The use of Raman spectroscopy to characterize double B/Z conformational junctions in DNA, J. Mol. Struct. 242 (1991) 135–141.

[55] W. Saenger, Principles of Nucleic Acid Structure, Ch. 1,6, 8, 14, Springer-Verlag, New York, 1984.

[56] S.S. Chan, K.J. Breslauer, R.H. Austin, M. Hogan, Thermodynamics and premelting conformational changes of phased $(dA)_5$ tracts, Biochemistry 32 (1993) 11776–11784.

[57] J.E. Herrera, J.B. Chaires, A premelting conformational transition in Poly(dA)–Poly(dT) coupled to daunomycin binding, Biochemistry 28 (1989) 1993–2000.

[58] J.D. Otvos, W.E. Antholine, S. Wherli, D.H. Petering, Metal coordination environment and dynamics in 113cadmium bleomycin: relationship to zinc bleomycin, Biochemistry 35 (1996) 1458–1465.

[59] A.M. Calafat, H. Won, L.G. Marzilli, A new arrangement for the anticancer antibiotics tallysomycin and bleomycin when bound to zinc: an assessment of metal and ligand chirality by NMR and molecular dynamics, J. Am. Chem. Soc. 199 (1997) 3656–3664.

[60] R.A. Manderville, J.F. Ellena, S.M. Hecht, Interaction of Zn(II) bleomycin with $d(CGCTAGCG)_2$. A binding model based on NMR experiments and restrained molecular dynamics calculations, J. Am. Chem. Soc. 117 (1995) 7891–7903.

[61] A. Toyama, N. Hanada, J. Ono, E. Yoshimitsu, H. Takeuchi, Assignments of guanosine UV resonance Raman bands on the basis of ^{13}C, ^{15}N and ^{18}O substitution effects, J. Raman Spectrosc. 30 (1999) 623–630.

[62] Q. Guo, M. Lu, M. Shahrestanifar, R.D. Sheardy, N.R. Kallenbach, Conformational properties of B–Z junctions in DNA, Biochemistry 30 (1991) 11735–11741.

[63] A. Ichikawa, T. Kuboya, T. Aoyama, Y. Sugiura, Activation of DNA cleavage by dynemicin A in a B–Z conformational junction, Biochemistry 31 (1992) 6784–6787.

[64] R.P. Hertzberg, M.J. Caranfa, S.M. Hecht, Degradation of structurally modified DNAs by bleomycin group antibiotics, Biochemistry 27 (1988) 3164–3174.

[65] R.S. Magliozzo, J. Peisach, M.R. Ciriolo, Transfer RNA is cleaved by activated bleomycin, Mol. Pharmacol. 35 (1989) 428–432.

[66] J.-M. Battigello, M. Cui, B.J. Carter, RNA recognition and cleavage by Fe(II) bleomycin, in: A. Sigel, H. Sigel (Eds.), Metal Ions in Biological Systems, 33, Marcel Dekker, New York, 1996, pp. 593–617.

[67] C.E. Holmes, S.M. Hecht, Fe bleomycin cleaves a transfer RNA precursor and its 'transfer DNA' analog at the same major site, J. Biol. Chem. 268 (1993) 25909–25913.

[68] B.J. Carter, E. de Vroom, E.C. Long, G.A. van der Marel, J.H. van Boom, C. Debouck, S.M. Hecht, Site-specific cleavage of RNA by Fe(II) bleomycin, Proc. Natl. Acad. Sci. USA 87 (1990) 9373–9377.

[69] R.D. Sheardy, N. Levine, S. Marotta, D. Suh, J.B. Chaires, A thermodynamic investigation of the melting of B–Z junction forming DNA oligomers, Biochemistry 33 (1994) 1385–1391.

[70] Z. Reich, P. Friedman, S. Levin-Zaidman, A. Minsky, Effects of adenine tracts on the B–Z transition, J. Biol. Chem. 268 (1993) 8261–8266.

[71] A. Herbert, A. Rich, The biology of left-handed Z-DNA, J. Biol. Chem. 271 (1996) 11595–11598.

[72] L.D. Williams, I.H. Goldberg, Selective strand scission by intercalating drugs at DNA bulges, Biochemistry 27 (1988) 3004–3011.

[73] I.D. Campbell, R.A. Dwek, Biological Spectroscopy, Ch. 4, Benjamin/Cummings Publishing, Reading, MA, 1984.